catalysts

MDPI

Article

Effect of Zirconia on Hydrothermally Synthesized Co_3O_4/TiO_2 Catalyst for NO_x Reduction from Engine Emissions

Muhammad Habib Ur Rehman [1], Tayyaba Noor [2] and Naseem Iqbal [1,*]

[1] U.S-Pakistan Center for Advanced Studies in Energy (USPCAS-E), National University of Sciences and Technology (NUST), H-12, Islamabad 44000, Pakistan; engr.habib952@gmail.com

[2] School of Chemical & Materials Engineering (SCME), National University of Sciences & Technology (NUST), H-12, Islamabad 44000, Pakistan; tayyaba.noor@scme.nust.edu.pk

* Correspondence: naseem@uspcase.nust.edu.pk

Received: 13 December 2019; Accepted: 8 January 2020; Published: 9 February 2020

Abstract: Effect of zirconia on the 6 wt.% Co_3O_4/TiO_2 catalyst for NO_x reduction is investigated in this paper. Co_3O_4/TiO_2 catalyst was prepared by using hydrothermal method and then was promoted with zirconia by impregnation to get 8% wt. ZrO_2-Co_3O_4/TiO_2 catalyst. Catalysts were characterized by using XRD, SEM, and TGA. Catalysts real time activity was tested by coating them on stainless steel wire meshes, containing them in a mild steel shell and mounting them at the exhaust tailpipe of a 72 cm^3 motorcycle engine. Zirconia promoted catalyst showed higher conversion efficiency of NO_X than the simple Co_3O_4/TiO_2 catalyst due to small crystalline size, fouling inhibition and thermal stability.

Keywords: Co_3O_4/TiO_2 catalyst; ZrO_2-Co_3O_4/TiO_2 catalyst; NO_X reduction; CO and HC oxidation

1. Introduction

Pollutant gas emission from automotive vehicles is one of the biggest contributors to air pollution in most cities of the world [1–4]. Annually, 4.2 million people die due to the ambient air pollution throughout the world [5,6]. Since the introduction of the clean air act in 1970, a number of efforts have been made to reduce the engine exhaust pollution. Engine exhaust emissions contain three major pollutants—carbon monoxide (CO), nitrogen oxides (NOx), and hydrocarbons (HCs)—which need to be tackled [7]. Different methods, such as thermal reactors, diesel particulate filters (DPFs), selective catalytic reduction SCR, changes in engine design, oxygenated fuels, and catalytic converters had been adopted to truncate this concern to the minimum level [4,8]. Gasoline blended with 3% oxygen by weight reduces 30% of CO emissions but NO_X concentration increases which can swell ozone problems [9]. Conventionally catalytic converters employ Pt, Pd, and Rh as catalysts with innovations, such as the introduction of CeO_2 or CeO_2-ZrO_2 composite for managing the time lag from switching between lean to rich condition or vice versa [10]. These metals are emitted out due to high temperatures, mechanical friction, stresses, and chemical reactions to the roadside soils which cause disruption in plant growth [11]. Due to high solubility of PGEs with various compounds, the presence of these metals in the environment can cause many health threats, such as nausea, tumors, sensitization, pregnancy loss and other human health issues [12,13]. Moreover, due to thermal aging, Rh_2O_3 reacts with Al_2O_3 to form an inactive compound, Pt sintering occurs at 700 °C and at high temperature of 900 °C sintering of γ-AL_2O_3 occurs and it transforms to α-AL_2O_3 which has less surface area [14]. These metals are rarest of the elements present on the earth ranging from 5 to 15 ppm in ores mines and from 0.022 ppb for Ir to 0.52 ppb for Pd [15,16]. The automotive industry consumed

37% of platinum, 72% of palladium and 79% of rhodium in 2013 [15]. Due to the scarcity of these metals, increasing prices and health hazards, it is a requirement to find a replacement which is less rare, less expensive, and competitively active. Over time, many pure metals and metal oxides were tested as alternatives to these PGEs for redox reactions in catalytic converters i.e., Au, Ni, Cu, MnO_2, CoO, Co_3O_4 and CuO [15,17–19]. Co_3O_4 over different supports was investigated as a catalyst for oxidation of CO and HC in exhaust emission control system and demonstrated low temperature activity [20,21]. Wang et al. [22] experimented by preparing a cobalt oxide catalyst with three different supports, such as TiO_2, Al_2O_3 and SiO_2 by using the incipient wetness impregnation method. He expressed that the type of cobalt oxide and type of support used had a great effect on the activity and the surface area. He concluded that CoO_x/TiO_2 showed very significant results towards CO conversion. Hu et al. [23] performed the oxidation of CO on cobalt oxides nanobelts and nanocubes. He revealed that the shape Co_3O_4 had a great effect on the catalytic activity towards CO as nanobelts depicted more conversion efficiency than nanocubes. Jia et al. [24] prepared Co_3O_4-SiO_2 nanocomposite as catalyst with high surface area for oxidation of CO. He observed that the catalyst showed activity at a very low temperature of even −76 °C. He concluded that there was some adsorption of water molecules on the exterior of catalyst which caused abnormal behavior in the activity of catalyst. Xie et al. [25] reported that Co_3O_4 showed high activity for carbon monoxide conversion surprisingly at temperature of −77 °C and remained stable under the moist conditions. He observed that under the stoichiometric conditions, conversion efficiency of Co_3O_4 catalyst was 96% at temperature of 200 °C but the conversion efficiency decreased at temperature of 150 °C to 40% due the presence of moisture content.

On the other hand, due to high thermal stability, high surface area, and highly resistant towards poisoning TiO_2 was widely used for catalyst support as an alternate to alumina [26,27]. Titanium dioxide exists in three crystalline phas.

es that are anatase, brookite, and rutile however anatase and rutile play a role in applications of titanium dioxide. Anatase is less dense and less stable than rutile at ambient temperature and pressure conditions [28]. Zhu et al. [29] studied the effect of TiO_2 structure on catalytic properties of copper oxide supported by anatase or rutile for NO reduction by CO reaction. He concluded that copper oxide supported by rutile TiO_2 was more active than supported by anatase TiO_2. Presently, commercially available three way catalysis systems have ceria or ceria-zirconia along with alumina and precious metal to increase the conversion efficiency. The incorporation of ceria-zirconia mixture into automotive catalysts was to enhance the oxygen storage capacity (OSC) for the redox reactions by releasing/storing oxygen depending upon A/F ratio and other factors [30]. Extensive studies were carried on ceria, zirconia, and a mixture of both as OSC is very important for the increment of CO oxidation as well as the reduction of NOx at the same time. Transition metal oxides showed a great potential to have oxygen vacancies on the surface like TiO_2, ZrO_2 and V_2O_5 [31]. Yu et al. [32] studied the adsorption and oxidation of CO by O_2 at the surface of rutile TiO_2. Li et al. [33] calculated the oxygen vacancies on anatase and rutile TiO_2 and concluded that both phases have oxygen vacancies but in case of rutile more stable oxygen vacancy was found on the surface rather on subsurface. In the case of zirconia, oxygen vacancies are produced by doping but undoped zirconia also contains bulk concentration of oxygen vacancies [34,35]. In this work, we are going to present the effect of zirconia on hydrothermally produced Co_3O_4/TiO_2 catalyst for petrol engine emissions control system with Co_3O_4 being our oxidation catalyst and TiO_2 as reduction catalyst. Zirconia was impregnated on a catalyst and a new 8% wt. ZrO_2-Co_3O_4/TiO_2 was prepared. Both catalysts were coated on round wire meshes then placed in a mild steel clam shell and mounted on the exhaust of a motorcycle. The zirconia promoted catalyst showed more qualities of reductive catalyst as less NO_x were seen after the reaction inside the catalytic converter.

2. Results and Discussions

2.1. X-ray Diffraction (XRD)

All phases of the prepared catalyst were identified by using JCPDS powder diffraction file. In XRD analysis of Co_3O_4/TiO_2, the phase of titania identified was rutile and no peaks of other phases of titania were noticed. XRD pattern of Co_3O_4/TiO_2 catalyst is shown in Figure 1a. TiO_2 showed peaks at 2 theta values of 27.45°, 36.06°, 41.22°, 44.04°, 54.31°, 56.6°, 62.7°, 64.03°, 69.008° and 69.78°. Diffraction peaks of rutile titania are in complete match with JCPDS card no. 21-1276. Crystallite size of titania nanoparticles was calculated by Sherrer equation which was 65 nm on average. TiO_2 exhibited tetragonal crystal structure with the cell parameters as a = 4.593 Å, b = 4.593 Å and c = 2.959 Å. In XRD analysis of the catalyst the cubic crystal structure of cobalt oxide Co_3O_4 was identified with the cell parameters a = 8.084 Å, b = 8.084 Å and c = 8.084 Å. The pattern in Figure 1a shows strong peaks at the 2 theta values of 19°, 31.2°, 36.84°, 44.85°, 55.6° and 65.2° for Co_3O_4 matching with JCPDS card no. 42-1467. Crystallite size of cobalt oxide was determined by using Sherrer equation which came out to be 26 nm. No other peaks of $Co(OH)_2$ or any impurity were observed. XRD pattern of 8 wt.% ZrO_2-Co_3O_4/TiO_2 is shown in Figure 1b. Co_3O_4, TiO_2 and ZrO_2 were detected successfully. Peaks of monoclinic crystal structure of zirconia (ZrO_2) were observed at 24.04°, 24.44°, 28.17°, 31.46°, 34.15°, 34.38°, 49.26° and 50.55°. Crystallite size of zirconia was calculated as 32 nm on average. In 8 wt% ZrO_2-Co_3O_4/TiO_2 crystallite size of TiO_2 and Co_3O_4 calculated by Sherrer equation decreased to 58 nm and 22 nm respectively as compared to Co_3O_4/TiO_2.

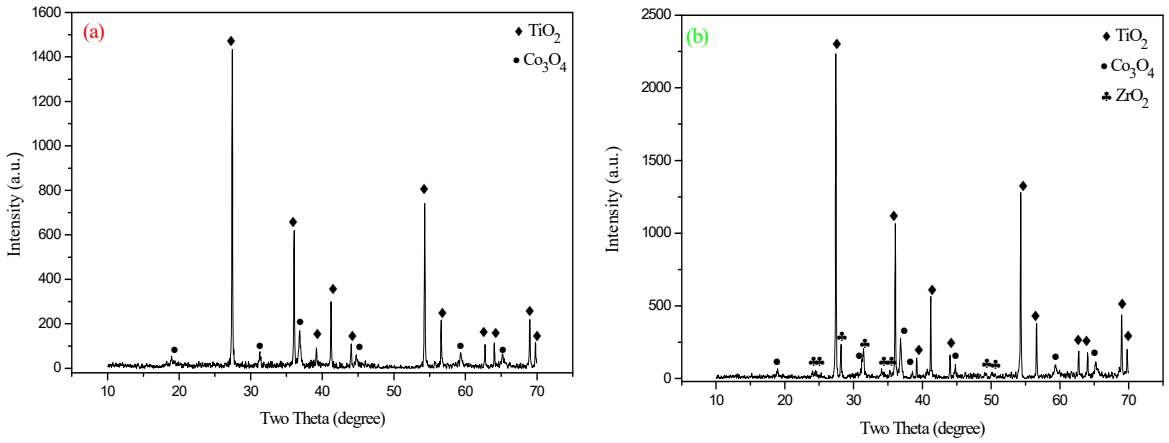

Figure 1. XRD patterns of catalysts (**a**) Co_3O_4/TiO_2 (**b**) 8% wt. ZrO_2-Co_3O_4/TiO_2.

2.2. Scanning Electron Microscopy (SEM)

SEM images of the samples are shown in Figure 2 with different scaling. It was observed that the particles of titania and both catalysts were spherical in shape and size, were in range of 50–170 nm. SEM images of titania nanoparticles and both catalysts are shown in Figure 2a–c. It was observed size and the shape of the particles were uniform without many variations. Titania nanoparticles image show that boundaries of particles are clear and well defined but after loading of Co_3O_4 clear structure starts diminishing. After addition of zirconia that smooth and well defined structure lessens very much. SEM images of a coated wire pieces before and after testing are shown in Figure 2d–g. Slight removal of the coated material was observed after testing and also there was some agglomeration of coated material after testing. This ascertains that coating technique needs to be upgraded. EDS (Energy-dispersive X-ray spectroscopy) patterns are shown in Figure 3. It was noticed in EDS analysis that there was no deposition of emission particles on coated wires with the catalysts after repetitive testing at varying conditions.

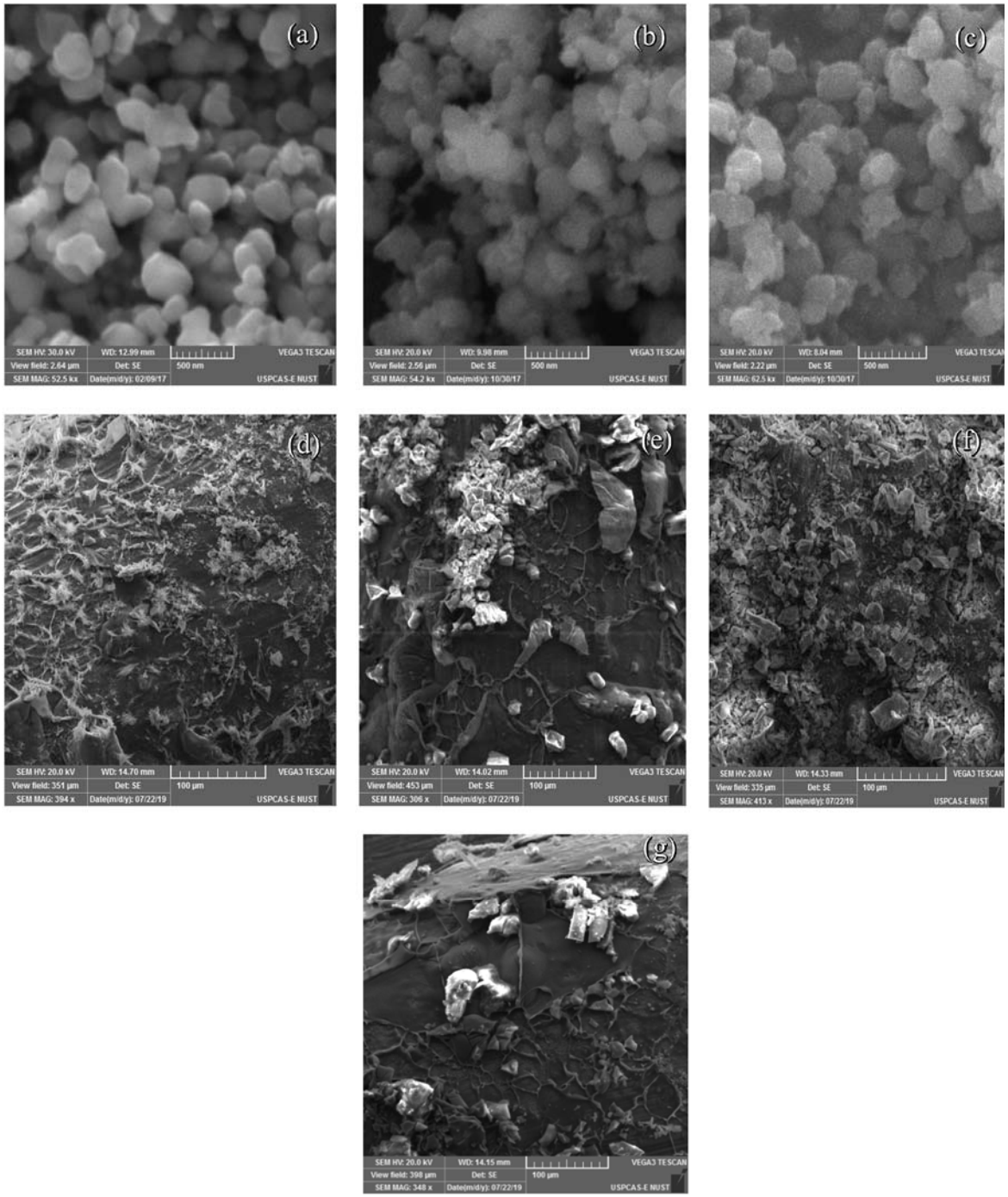

Figure 2. SEM images of (**a**) TiO_2 nanoparticles (**b**) Co_3O_4/TiO_2 (**c**) 8 wt.% ZrO_2-Co_3O_4/TiO_2 (**d**) Bef test 8 wt.% ZrO_2-Co_3O_4/TiO_2 coated wire (**e**) Aft test 8 wt.%. ZrO_2-Co_3O_4/TiO_2 coated wire (**f**) Bef test 8 wt.% ZrO_2-Co_3O_4/TiO_2 coated wire (**g**) Aft test 8 wt.% ZrO_2-Co_3O_4/TiO_2.

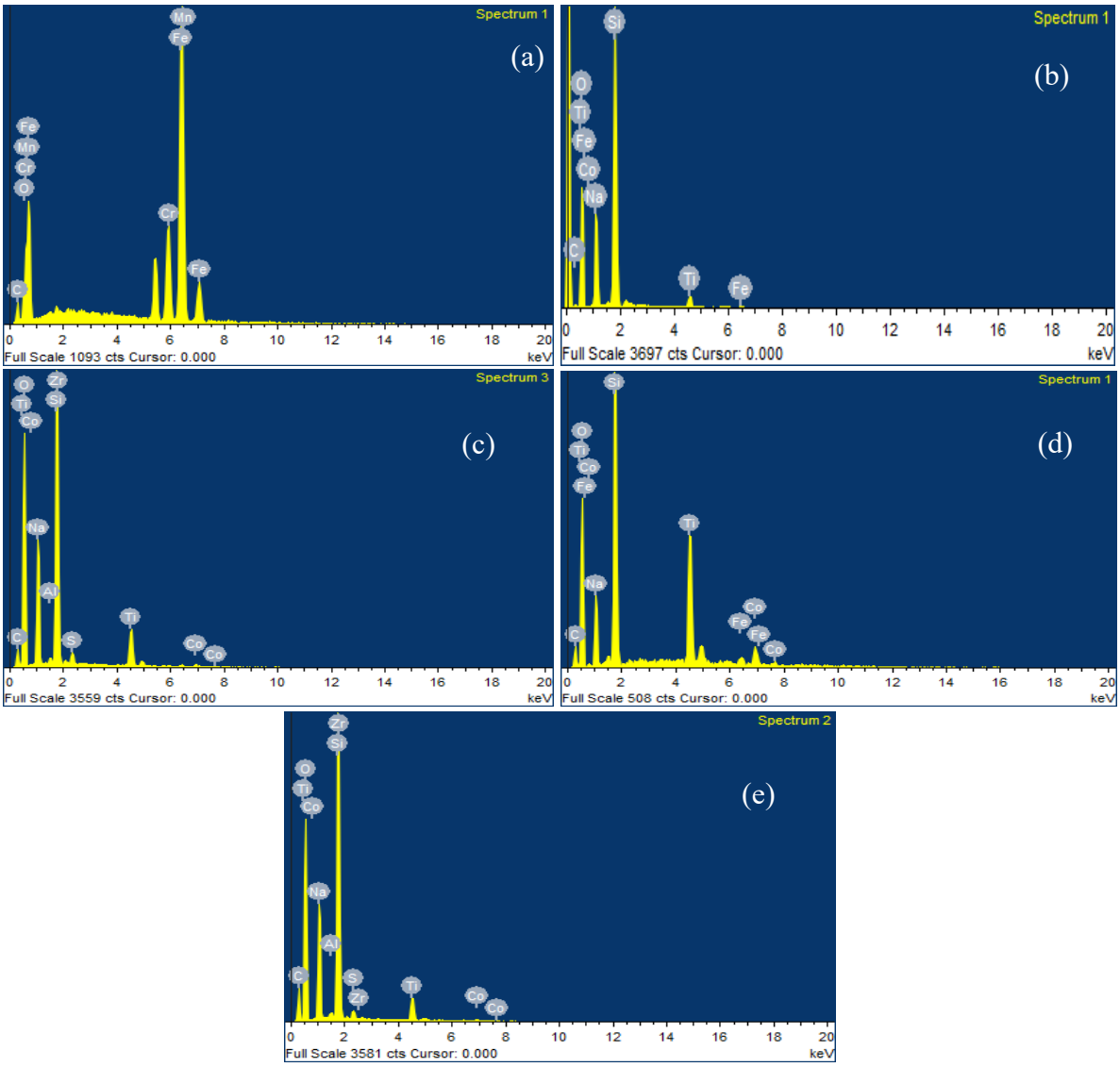

Figure 3. EDS patterns of (**a**) Uncoated wire (**b**) Co_3O_4/TiO_2 coated wire before test (**c**) 8 wt.% ZrO_2-Co_3O_4/TiO_2 coated wire before test (**d**) Co_3O_4/TiO_2 coated wire after test (**e**) 8 wt.% ZrO_2-Co_3O_4/TiO_2 coated wire after test.

2.3. Thermogravimetric Analysis (TGA)

Cyclic heating and cooling technique was carried out to find out the oxygen storage capacity (δ) of both catalysts as shown in Figure 4a,b. During real driving conditions when vehicle is accelerated, AFR fluctuates due to which NO_X emissions are increased. CeO_2 was used in conventional three way catalysts to overcome this fluctuating AFR issue as it has the ability to store/release oxygen during varying conditions. Zirconia with different mole fractions was added to give thermal stability and decrease sintering of CeO_2 [36]. In our case, we added 8 wt.% ZrO_2 in Co_3O_4/TiO_2 catalyst and investigated its effects on thermal stability and oxygen storage capacity of the catalyst. For this purpose, catalysts powders were put in the furnace of a TG analyzer turn by turn. Powders were heated from room temperature to 800 °C in the presence of air stream to provide atmospheric conditions with flow rate of 10 mL/min. Weight loss in the first heating cycle was calculated as 6.84% for Co_3O_4/TiO_2 catalyst and 7.22% for 8 wt.% ZrO_2-Co_3O_4/TiO_2 which corresponds to both loss of water and also oxygen molecules [37,38]. From 28 °C to 105 °C zirconia promoted catalyst lost 2.21% of weight while other catalyst experienced 0.51% of weight loss which indicates loss of moisture. After that, zirconia

promoted catalyst exhibited more stability and lost 5.03% weight compared to 6.67% of simple catalyst. Then, they were cooled to 169 °C in the presence of an air stream with same flow during which zirconia promoted catalyst gathered 1.87% and simple catalyst gathered 3.37% of weight which corresponds to oxygen gaining of both catalysts [36]. The OSC value (δ) of zirconia promoted catalyst was calculated to be 1.4 μmol/g and for simple catalyst it was 1.6 μmol/g which are quite significant values as per literature [39]. The zirconia promoted catalyst displayed less oxygen storage capacity which is due to crystal structural defects; the introduction of Zr into a Co framework on a corresponding level would compensate the volume increase related to Co^{2+} reduction. This would decrease the influence of valence change; shorten the Co-O bond length in the ZrO_2-Co_3O_4/TiO_2 as a result it detains some of oxygen sites on cobalt oxide and titania [40]. There was 3.54% weight loss observed for simple catalyst in second heating cycle while zirconia promoted catalyst lost 2.2% weight as shown in Figure 4a,b which corresponds to the oxygen releasing capacity of the catalysts in atmospheric conditions. Results of TGA show that with addition of zirconia, which is highly stable molecule, catalyst gained thermal stability but oxygen gaining and releasing ability decreased which also affected the catalytic activity that is discussed in later part of the paper. A decrease in crystalline size was observed by addition of ZrO_2 on Co_3O_4/TiO_2, which may attribute to increase in thermal stability of ZrO_2-Co_3O_4/TiO_2. Hofmann et al. [31] studied oxygen vacancies on rutile TiO_2 (both active catalyst and support) and reported that it has significant ability to store and release oxygen. After addition of the zirconia in Co_3O_4/TiO_2 catalyst, it captures some of oxygen vacant sites of titania which results in a lower OSC value.

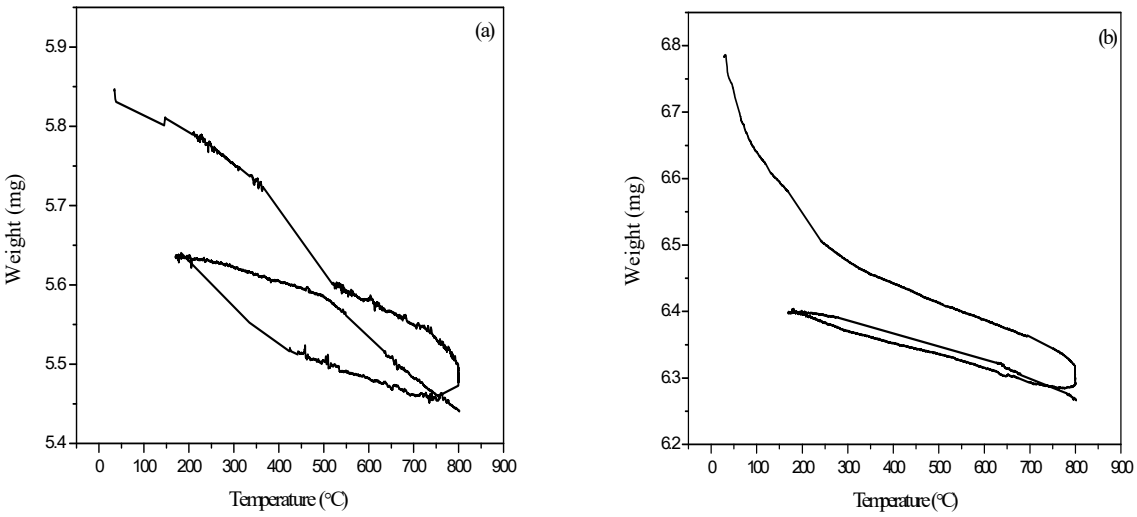

Figure 4. Plots for measurements of oxygen storage capacity (OSC) of (**a**) Co_3O_4/TiO_2 and (**b**) 8 wt.% ZrO_2-Co_3O_4/TiO_2.

2.4. Brunauer–Emmett–Teller (BET)

The surface area and pore volume for the Co_3O_4/TiO_2 catalyst were found to be 24.3 m^2/g and 0.14 cm^3/g, respectively, while the zirconia promoted catalyst surface area and pore volume were found to be 13.09 m^2/g and 0.071 cm^3/g, respectively. Reason behind decrement in surface area of zirconia promoted catalyst is that ZrO_2 which has higher density (5.68 gcm^{-3}) than titania, exhibits low surface area which is because of defects in crystal structural. This would decrease the influence of valence change; shorten the Co-O bond length in the ZrO_2-Co_3O_4/TiO_2, as a result it detains some of oxygen sites on cobalt oxide and titania may results in low surface area and low pore volume [41,42]. The N_2 adsoption-desorption isotherm of both catalysts is shown in Figure 5a,b.

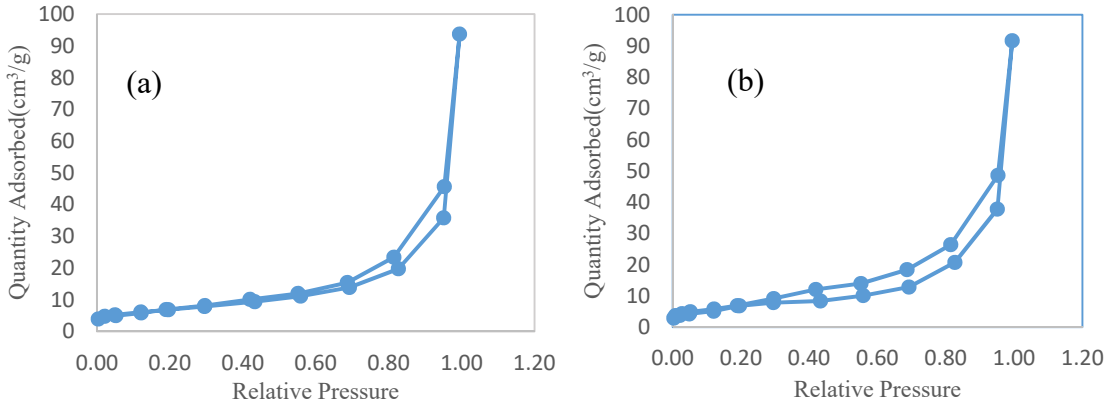

Figure 5. Nitrogen adsorption-desorption isotherm of (**a**) Co_3O_4/TiO_2 catalyst (**b**) 8 wt.% ZrO_2-Co_3O_4/TiO_2 catalyst.

2.5. Catalytic Activity

RPMs of the engine shaft increased manually from 1500 to 6000 at intervals of 1500. Temperature of the exhaust gases also increased giving values 121 °C, 257 °C, 284 °C, and 391 °C with respect to RPMs of 1500, 3000, 4500, and 6000. In the case of NO_X the maximum conversion efficiency was noticed at 6000 RPMs as shown in Figure 6 which was 71.4% for simple catalyst but zirconia promoted catalyst showed higher efficiency of 75% for NO_X reduction shown in Figure 7. The highest efficiency of zirconia promoted catalyst is due to absence of moisture content at high temperature, the poisoning of catalyst was diminished when temperature reach above 300 °C thus it provides more sites for reaction. Furthermore, NO_X amount in the gas stream was maximum in its range. While lambda value at this point was 1.323 which showed that the air to fuel ratio (AFR) inside the combustion chamber of motorcycle engine was 19.5:1 and the air fuel mixture was lean. Shah et al. [40] coated wire meshes with zirconia and reported that it reduced HCs in exhaust stream by 35%. In the case of CO, maximum conversion efficiency was noticed at 1500 RPMs which was 78.15% for simple catalyst shown in Figure 8 and slightly higher 78.65% for zirconia promoted catalyst as shown in Figure 9. CO oxidation is strongly dependent on morphology of catalysts and oxidation state of transition metals in catalyst. The oxidation state of Co in the prepared Co_3O_4/TiO_2 and ZrO_2-Co_3O_4/TiO_2 was expected to be +2 in both cases with tetrahedral and octahedral geometries respectively. Despite similar Co coordination environments, the catalytic activity and selectivity was considerably improved by the Zr modification of the Co_3O_4/TiO_2. This was endorsed to the change in oxygen donor ability and Co–O bond strength of the ≡TiO–Zr–O sites of Co–Zr/TiO_2 compared with the ≡TiO– ligands in Co/TiO_2. The tuning of the support TiO_2 oxygen donation ability by use of an anchoring site (e.g., ≡TiO–Zr–O^-) can be used to alter both rate and selectivity of conversion efficiency i.e., (NO_x, CO, HC). Possibly Co^{2+} active sites prefer to associate with ≡TiO–Zr–O^- sites as compare to ≡TiO– [42,43] as shown in below Figure 10. Furthermore, zirconia promoted catalyst efficiency is attributed by the presence of zirconia that effect on redox properties through dispersion of active phases which oxidize CO more efficiently. Moreover, at this point CO amount in exhaust gas was maximum in its range which decreases drastically with temperature increment from 1500 to 6000 RPMs. The inlet lambda value was noticed to be same 1.323 thus the AFR value of 19.5:1. Higher AFR indicating that air fuel mixture is lean thus oxidation reactions are more favorable. The outlet lambda value after the catalyst was recorded as 6.02 which mean that catalyst is working properly.

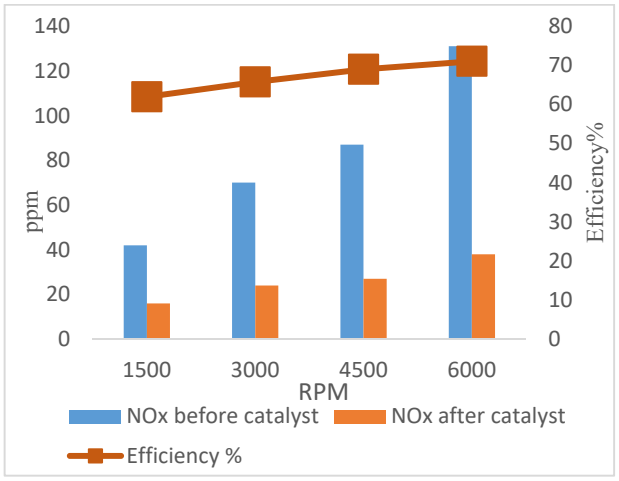

Figure 6. Conversion of NO_X with Co_3O_4/TiO_2.

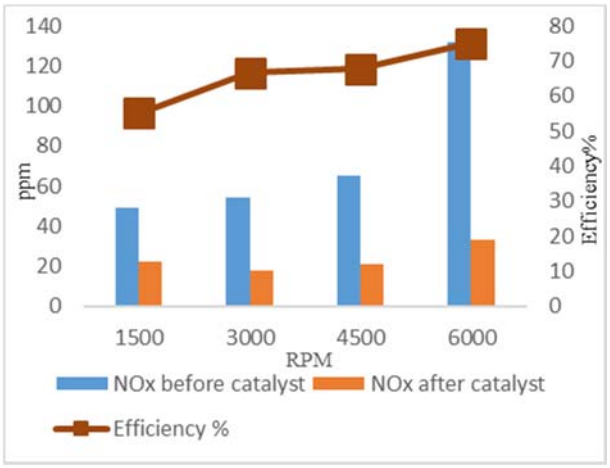

Figure 7. Conversion of NO_X with 8 wt.% ZrO_2-Co_3O_4/TiO_2.

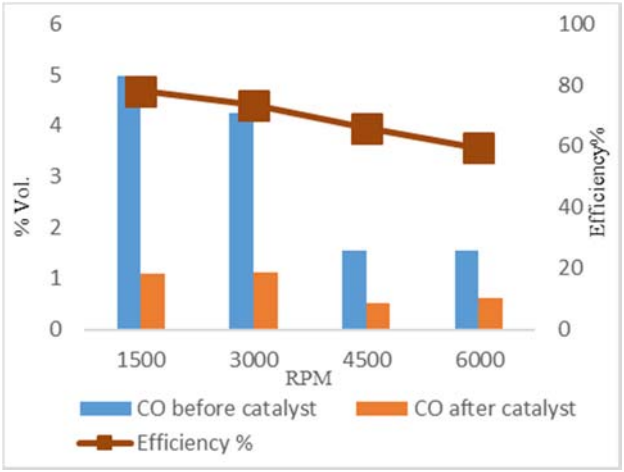

Figure 8. Conversion of CO with Co_3O_4/TiO_2.

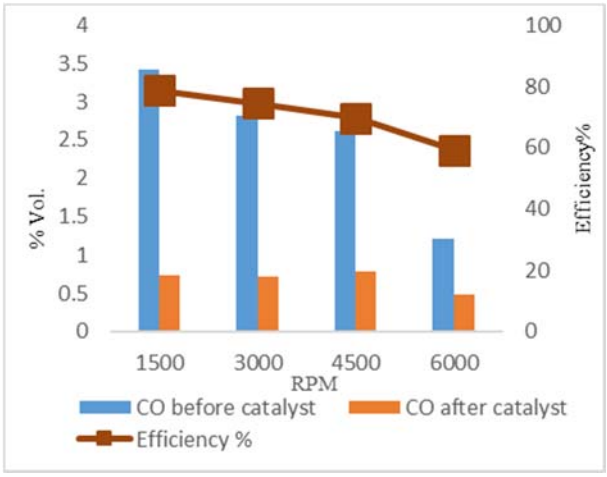

Figure 9. Conversion of CO with 8 wt.% ZrO_2-Co_3O_4/TiO_2.

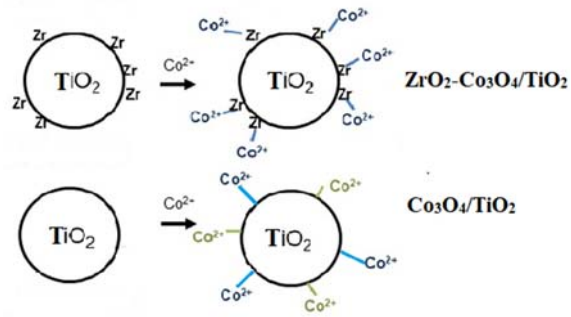

Figure 10. Graphical diagram of 8 wt.% ZrO_2-Co_3O_4/TiO_2 and Co_3O_4/TiO_2.

Furthermore, the type of basic sites together with whole basicity and whole acidity of the ZrO_2-based catalysts also effect the HC, CO, and NO_x conversion on active sites. The Lewis basic sites of ZrO_2 consist of coordinately unsaturated O^{-2} species and the Lewis acidic sites is Zr^{4+} species [42–46]. Overall reactions on the surface of catalysts were given below in Figure 11:

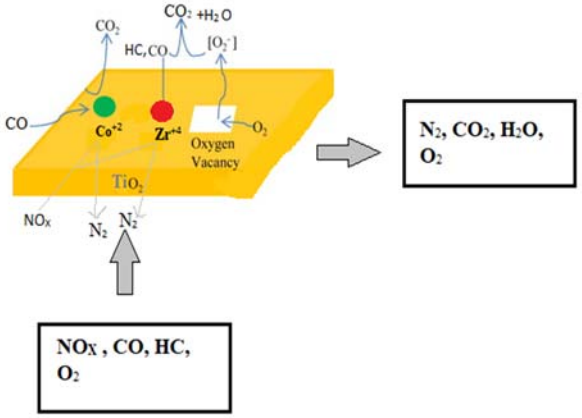

Figure 11. Conversions of NO_x, CO, HC to N_2, CO_2, and H_2O on 8 wt.% ZrO_2-Co_3O_4/TiO_2.

Amin et al. [39] developed a copper-based catalytic converter and reported that it converted HCs by 33% and CO by 66% at full load. Patel et al. [47] made a copper-based catalytic converter and reported conversion efficiencies as 50–62% for CO, 20–27% for NO_X and 35–40% HCs. Makwana et al. fabricated a catalytic converter by coating nickel on steel wire meshes and reported efficiencies as 40% and 35% for HCs, and CO, respectively. Hydrocarbons conversion efficiency was noticed as

82.5% for simple catalyst at 1500 RPMs as shown in Figure 12 but in case of promoted catalyst HC conversion decreased and gave highest value of 81% shown in Figure 13. The decrease in efficiency is due to presence of moisture content that absorb very easily on the Lewis acid site of the catalyst at a lower temperature i.e., 121 °C, As a result it lowers the vacancies of oxygen for oxidation on zirconia promoted Co_3O_4. Furthermore, the zirconia promoted catalyst displayed less oxygen storage capacity which is due to zirconia captures some of oxygen sites on cobalt oxide and titania. Enhanced catalytic performance of ZrO_2 promoted catalyst may be attributed to small crystalline size (calculated by the sSherrer equation). As crystalline small decrease, the no of catalytic active sites increases accordingly. Therefore, it leads to the better conversion efficiency of the reactants towards product formation. Also due to increase in thermal stability of ZrO_2 promoted catalyst at higher temperatures, catalyst becomes more resistance towards sintering process which could lead to better catalytic performance. ZrO_2 is also reported to prevent deactivation of catalyst in catalytic converters, which is caused by fouling process due to incomplete combustion of fuel. The catalytic activity results are summarized in Tables 1–3.

Table 1. Real time conversion results of NO_X with both catalysts.

RPM	NO_X (ppm) for Co_3O_4/TiO_2	-		NO_X (ppm) for 8 wt.% ZrO_2- Co_3O_4/TiO_2	-	
-	Before	After	Efficiency (%)	Before	After	Efficiency (%)
1500	42	16	61.9	49	22	55.1
3000	70	24	65.7	54	18	66.6
4500	87	27	69.8	65	19	70.7
6000	131	38	71	132	33	75

Table 2. Real time conversion results of CO with both catalysts.

RPM	CO (% vol.) for Co_3O_4/TiO_2	-		CO (% vol.) for 8 wt.% ZrO_2- Co_3O_4/TiO_2	-	
-	Before	After	Efficiency (%)	Before	After	Efficiency (%)
1500	4.99	1.09	78.1	3.42	0.73	78.6
3000	4.24	1.13	73.3	2.82	0.72	74.8
4500	1.55	0.53	65.8	2.47	0.79	68
6000	1.51	0.63	58.2	1.2	0.49	59.1

Table 3. Real time conversion results of HCs with both catalysts.

RPM	HCs (ppm) for Co_3O_4/TiO_2	-		HCs (ppm) for 8 wt.% ZrO_2- Co_3O_4/TiO_2	-	
-	Before	After	Efficiency (%)	Before	After	Efficiency (%)
1500	414	72	82.6	418	78	81.3
3000	198	45	77.2	237	56	76.3
4500	124	38	69.3	128	42	67.1
6000	39	15	61.5	40	14	65

With increasing RPMs, the temperature also increased and the ppm value of hydrocarbons production inside combustion chamber decreased. Thus, confirming that amount of CO, NOx and HCs producing inside combustion chamber heavily depends on the temperature inside combustion chamber.

After addition of zirconia in catalyst, there was a negative effect on oxidation reactions as it suppressed the oxidation reaction of HCs. HC conversion efficiency was less in ZrO_2 promoted catalyst compared to the other one. This is because zirconia captures some of the active sites of Co_3O_4 which is our oxidation catalyst. Moreover, mostly transition metals oxides have the tendency to work as reduction catalysts [48]. TiO_2 was used as our reduction catalyst for NO_X, so addition of ZrO_2 itself

being a metal oxide which develops the reduction property at higher energies, contributed towards NOx reduction. It should be noted that about (50%–80%) of HCs are emitted during the cold start period which is about 200 s from the starting of an engine [49].

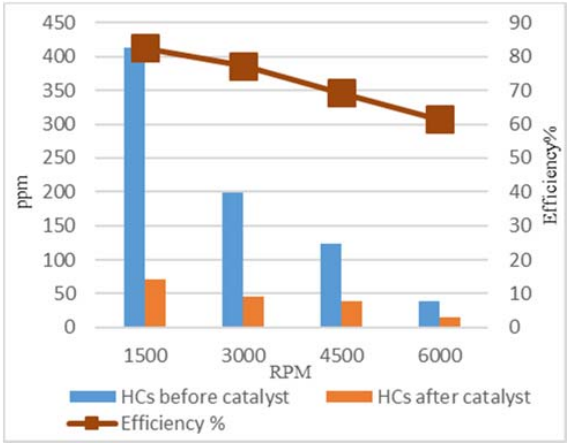

Figure 12. HC Conversions with Co_3O_4/TiO_2.

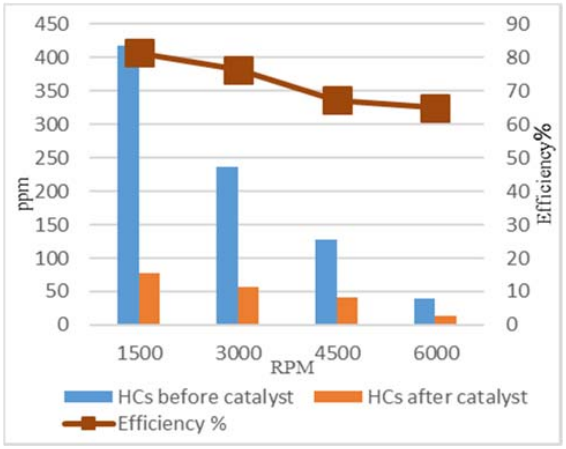

Figure 13. HC conversions with 8 wt.% ZrO_2- Co_3O_4/TiO_2.

Therefore, a good catalytic converter should convert maximum unburnt hydrocarbons during this span of time, maintained its high metal dispersion and high catalytic activity. In our case, both the catalysts showed maximum conversion efficiency for HCs in the beginning at the lowest RPMs. Uncoated wires mesh showed zero conversion of gases.

3. Experimental Section

3.1. Catalyst Preparation

For synthesis of TiO_2 nanoparticles, 60 g of titania powder (BDH) was added 400 mL of distilled water. The mixture was stirred for 24 h at 800 rpm and then it was allowed to settle down for 12 h. Then settled material was dried in oven for 12 h at 100 °C. The dried material was continuously crushed by using a pestle and mortar and then it was allowed to calcine at 500 °C for 6 h in a furnace. Co_3O_4/TiO_2 Catalyst was prepared by using hydrothermal synthesis method. For that purpose, 2.75 g of cobalt nitrate hexahydrate $Co(NO_3)_2.6H_2O$ (Panreac, Barcelona, Spain) was added to 30 mL of distilled water while stirring at room temperature to give 6 wt.% loading of Co_3O_4 over TiO_2 support. A mixture of potassium hydroxide KOH and water was added dropwise as precipitating agent for the formation of $Co(OH)_2$. The color of the mixture changed from pink to purple after addition of KOH. The pH value

of the solution was continuously monitored while adding KOH so that it should reach 8. Because as per literature [36] pH value from 8–9 gives a uniform size of Co_3O_4 while increasing pH to 11 or 12 give an irregular shape. Moreover, the condensation of $Co(OH)_2$ occurs at higher pH value due to which there are substantial chances of agglomeration of nanoparticles. After that, a 30% mass fraction of H_2O_2 (DAEJUNG, Busan, South Korea) was added dropwise in the solution as oxidant to convert $Co(OH)_2$ into spinel Co_3O_4 [36]. Color of the mixture started turning into brown from purple after addition of hydrogen peroxide. 4 g of titania nanoparticles were stirred in 40mL of water for one hour and then poured into a stainless steel autoclave along with the suspension already prepared. The autoclave was sealed and was put in a furnace at 180 °C for 10 h. Distilled water and ethanol were respectively used to wash the obtained material from autoclave and then it was dried in an oven at 100 °C for 8 h. 8% wt. zirconia (UNI-CHEM, Belgrade, Serbia) which is 0.15 g for 1 g of Co_3O_4/TiO_2 catalyst, was dissolved in required amount of distilled water and was dropped on the already prepared Co_3O_4/TiO_2 catalyst so that it completely soaked the powder. Then it was kept in oven at 100 °C for 5 h and calcined at 400 °C for 6 h to have 8% wt. ZrO_2-Co_3O_4/TiO_2.

3.2. Characterization

Powder X-ray diffraction (XRD) patterns were recorded by using Bruker D8 (Karlsruhe, Germany) Advance using Cu-kα radiation operating at 40 kV and 30 mA with 0.02° step size. Samples were scanned ranging the 2θ values from 10° to 70°. Tescan Vega3 scanning electron microscope (Brno, Czech Republic) was used to analyze the morphology of prepared catalysts and coated wires operating at 20 kV. Schimadzu DTG-60H (Kyoto, Japan) with an alumina pan was used to analyze the thermal stability and the oxygen storage capacity (OSC) of the zirconia promoted catalyst with temperature ranging from 28 °C to 800 °C with heating and cooling rate of 10 °C/min. Brunauer–Emmett–Teller (BET) surface areas of both catalysts were studied using N_2 adsorption and desorption isotherms with the help of Quantachrome, NOVA 2200e at −195.8 °C. Samples were degassed in vacuum at 300 °C for 3 h.

3.3. Fabrication and Testing of Catalytic Converter

3.3.1. Preparation of Wire Meshes

A SS-304 wire mesh sheet of 4 × 4 feet size was cut into 48 circular pieces of 6 cm diameter each as shown in Figure 14 by using a manual table cutter. Before coating the catalyst on the wire meshes, they were pretreated with 10% HCL. For this purpose wire meshes were kept dipping in 10% HCL for half an hour. After that distilled water was used to wash them and kept in an oven for drying for an hour at 100 °C. In this way, impurities were removed from the stainless steel structure. Cell density of wire meshes was 64 cells per square inch.

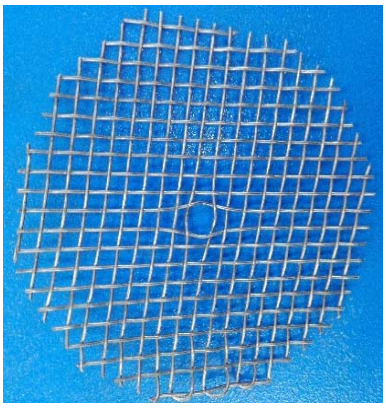

Figure 14. Wire mesh piece.

3.3.2. Catalyst Slurry

Catalyst slurry was prepared for coating it onto the wire mesh substrate. For this purpose, 3 g sodium metabisulfite (BDH) and 270 g of sodium silicate solution (Sigma-Aldrich, St. Louis, MI, USA) were added together for each catalyst separately while stirring shown in Figure 15. 30 g of each catalyst was added to this mixture and stirred for 12 h then it was coated on wire meshes.

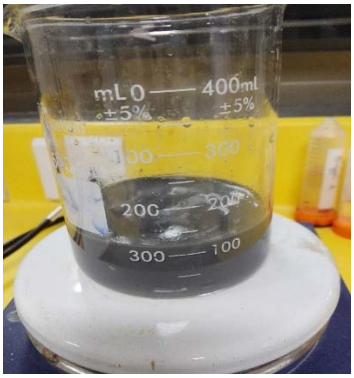

Figure 15. Catalyst slurry preparation.

3.3.3. Catalyst Coating

30 g of each catalyst was deposited on the pretreated wire meshes by using the dip coating method. After immersing, a blower was used to remove the extra material from the wires of structure. This immersion and blowing was repeated three times to achieve uniformity. The coated wire meshes were calcined in a furnace for 5 h at 400 °C to remove the impurities and then cooled at the room temperature.

3.3.4. Wire Meshes Arrangement

24 circular wire meshes (for each catalyst) after being coated were arranged on a threaded bar with 4 mm diameter with 1mm thick washers between them to keep them away from intermingling. Both sides of the bar were closed by using hexagonal nut. These catalysts coated wire mesh structures were respectively placed in mild steel clam shell as shown in Figure 16 for activity testing with an inner diameter of 6.2 cm and sealed with Teflon lining to prevent any leakage of gases.

Figure 16. Coated wire meshes arrangement

3.4. Activity Test

The fabricated catalytic converters were mounted at the exhaust pipe of a 70 cc petrol engine as shown in Figure 17 with 72 cm^3 displacement, 47 mm bore, and 41.4 mm stroke length was used. Test readings were taken by using Crypton's gas analyzer (Birmingham, UK) for CO and HC conversions

but for NO_x readings E instruments' E4500-2 was used. Catalytic activity readings were taken at 1500, 3000, 4500, and 6000 revolutions per minute which were manually set. Engine shaft angular speed was measured by a DT-2234B photo type digital tachometer.

Figure 17. Catalytic converter mounted on engine exhaust for testing

4. Conclusions

Two alternative catalysts, Co_3O_4/TiO_2 and 8% wt. ZrO_2 -Co_3O_4/TiO_2 along with a wire mesh-based substrate, were successfully developed and found very active for CO, HC, and NO_X conversions. Zirconia promoted catalyst showed more promising towards NO_X conversion. The cobalt supported by the titania Co_3O_4/TiO_2 catalyst shows a performance towards conversion of carbon monoxide, nitrogen oxides and unburnt hydrocarbons to a value of 78.1%, 61.9%, and 82.6% efficiency at 1500 RPM. Whereas, the conversion efficiency of zirconia promoted ZrO_2 -Co_3O_4/TiO_2 catalyst is 81.3%, 78.6%, and 55.1% towards HCs, CO, and NOx respectively at 1500 RPM value. Due to small crystalline size, thermal stability, and fouling inhibition, the ZrO_2 promoted Co_3O_4/TiO_2 catalyst showed better conversion efficiency towards CO and NOx. The slightly lower efficiency of zirconia promoted catalyst towards HCs is due to the non-availability of the vacancies of oxygen for oxidation on Co_3O_4. Both the catalysts showed selectivity towards CO, NO_X and HC and have comparable performance with respect to be the activity of a conventional catalyst.

Author Contributions: Conceptualization, M.H.U.R., T.N. and N.I.; data curation, methodology, and investigation, M.H.U.R.; supervision T.N., and N.I.; original draft preparation, M.H.U.R., T.N. and N.I.; writing—reviews and editing, all authors. All authors have read and agreed to the published version of the manuscript.

Funding: This research received no external funding.

Acknowledgments: U.S-Pakistan Center for Advanced Studies in Energy (USPCAS-E) at National University of Sciences and Technology (NUST) is highly acknowledged by authors for providing lab facilities.

Conflicts of Interest: The authors declare no conflict of interest.

References

1. Xia, T.; Nitschke, M.; Zhang, Y.; Shah, P.; Crabb, S.; Hansen, A. Traffic-related air pollution and health co-benefits of alternative transport in Adelaide, South Australia. *Environ. Int.* **2015**, *74*, 281–290. [CrossRef] [PubMed]
2. Cheng, Y.; Fan, Y.; Pei, Y.; Qiao, M. Graphene-supported metal/metal oxide nanohybrids: Synthesis and applications in heterogeneous catalysis. *Catal. Sci. Tech.* **2015**, *5*, 3903–3916. [CrossRef]
3. Lelieveld, J.; Evans, J.S.; Fnais, M.; Giannadaki, D.; Pozzer, A. The contribution of outdoor air pollution sources to premature mortality on a global scale. *Nature* **2015**, *525*, 367. [CrossRef] [PubMed]
4. Seigneur, C. *Air Pollution: Concepts, Theory, and Applications*; Cambridge University Press: Cambridge, UK, 2019.
5. World Health Organization. *World Health Statistics 2016: Monitoring Health for the SDGs Sustainable Development Goals*; World Health Organization: Washington, DC, USA, 2016.

6. Franco, V.; Kousoulidou, M.; Muntean, M.; Ntziachristos, L.; Hausberger, S.; Dilara, P. Road vehicle emission factors development: A review. *Atmos. Environ.* **2013**, *70*, 84–97. [CrossRef]
7. Lee, S.E. ARCHEOLOGY: Temple Gateways in South India: The Architecture and Iconography of the Cidambaram Gopuras. James, C.; Harle. *Am. Anthropol.* **1964**, *66*, 1445–1446. [CrossRef]
8. Cooper, C.D.; Alley, F.C. *Air Pollution Control: A Design Approach*, 4th ed.; Waveland Pr Inc.: Long Grove, IL, USA, 2010.
9. Schifter, I.; Gonzalez, U.; Diaz, L.; Sánchez-Reyna, G.; Mejía-Centeno, I.; González-Macías, C. Comparison of performance and emissions for gasoline-oxygenated blends up to 20 percent oxygen and implications for combustion on a spark-ignited engine. *Fuel* **2017**, *208*, 673–681. [CrossRef]
10. Gallini, N.T. The economics of patents: Lessons from recent US patent reform. *J. Econ. Perspect.* **2002**, *16*, 131–154. [CrossRef]
11. Zereini, F.; Wiseman, C.L. *Platinum Metals in the Environment*; Springer: Berlin/Heidelberg, Germany, 2015.
12. Wang, Y.; Li, X. Health risk of platinum group elements from automobile catalysts. *Procedia Eng.* **2012**, *45*, 1004–1009. [CrossRef]
13. LaMer, V.K.; Dinegar, R.H. Theory, production and mechanism of formation of monodispersed hydrosols. *J. Am. Chem. Soc.* **1950**, *72*, 4847–4854. [CrossRef]
14. Xu, Q.; Kharas, K.C.; Croley, B.J.; Datye, A.K. The contribution of alumina phase transformations to the sintering of Pd automotive catalysts. *Top. Catal.* **2012**, *55*, 78–83. [CrossRef]
15. Escrig-Olmedo, E.; Rivera-Lirio, J.M.; Muñoz-Torres, M.J.; Fernández-Izquierdo, M.Á. Integrating multiple ESG investors' preferences into sustainable investment: A fuzzy multicriteria methodological approach. *J. Clean. Prod.* **2017**, *162*, 1334–1345. [CrossRef]
16. Mudd, G.M.; Jowitt, S.M.; Werner, T.T. Global platinum group element resources, reserves and mining—A critical assessment. *Sci. Total Environ.* **2018**, *622*, 614–625. [CrossRef] [PubMed]
17. Scurrell, M.S. Thoughts on the use of gold-based catalysts in environmental protection catalysis. *Gold Bull.* **2017**, *50*, 77–84. [CrossRef]
18. Zhao, F.; Harrington, D.L.; Lai, M.-C. *Automotive Gasoline Direct-Injection Engines*; Society of Automotive Engineers: Warrendale, PA, USA, 2002; Volume 400.
19. Guerrero, L.M.; Mendoza, J.F.; Ong, K.T.V.; Olegario-Sanchez, E.M.; Ferrer, E.L. Copper-Exchanged Philippine Natural Zeolite as Potential Alternative to Noble Metal Catalysts in Three-Way Catalytic Converters. *Arab. J. Sci. Eng.* **2019**, *44*, 5581–5588. [CrossRef]
20. Li, L.; Yao, Y.; Tang, Z.; Ji, W.; Dai, Y.; Shen, X. Size Effect of Co3O4 Nanoparticles as Catalysts for CO Oxidation. *J. Nanosci. Nanotechnol.* **2016**, *16*, 7573–7578. [CrossRef]
21. Ma, L.; Seo, C.Y.; Chen, X.; Sun, K.; Schwank, J.W. Indium-doped Co3O4 nanorods for catalytic oxidation of CO and C3H6 towards diesel exhaust. *Appl. Catal. B Environ.* **2018**, *222*, 44–58. [CrossRef]
22. Wang, C.-B.; Tang, C.-W.; Tsai, H.-C.; Chien, S.-H. Characterization and catalytic oxidation of carbon monoxide over supported cobalt catalysts. *Catal. Lett.* **2006**, *107*, 223–230. [CrossRef]
23. Teng, Y.; Kusano, Y.; Azuma, M.; Haruta, M.; Shimakawa, Y. Morphology effects of Co 3 O 4 nanocrystals catalyzing CO oxidation in a dry reactant gas stream. *Catal. Sci. Tech.* **2011**, *1*, 920–922. [CrossRef]
24. Jia, C.-J.; Schwickardi, M.; Weidenthaler, C.; Schmidt, W.; Korhonen, S.; Weckhuysen, B.M.; Schüth, F. Co3O4–SiO2 nanocomposite: A very active catalyst for CO oxidation with unusual catalytic behavior. *J. Am. Chem. Soc.* **2011**, *133*, 11279–11288. [CrossRef]
25. Xie, X.; Li, Y.; Liu, Z.-Q.; Haruta, M.; Shen, W. Low-temperature oxidation of CO catalysed by Co 3 O 4 nanorods. *Nature* **2009**, *458*, 746. [CrossRef]
26. Yao, X.; Zhao, R.; Chen, L.; Du, J.; Tao, C.; Yang, F.; Dong, L. Selective catalytic reduction of NOx by NH3 over CeO2 supported on TiO2: Comparison of anatase, brookite, and rutile. *Appl. Catal. B Environ.* **2017**, *208*, 82–93. [CrossRef]
27. Xu, W.; Yu, Y.; Zhang, C.; He, H. Selective catalytic reduction of NO by NH3 over a Ce/TiO2 catalyst. *Catal. Commun.* **2008**, *9*, 1453–1457. [CrossRef]
28. Rui, Z.; Wu, S.; Peng, C.; Ji, H. Comparison of TiO2 Degussa P25 with anatase and rutile crystalline phases for methane combustion. *Chem. Eng. J.* **2014**, *243*, 254–264. [CrossRef]
29. Zhu, H.; Dong, L.; Chen, Y. Effect of titania structure on the properties of its supported copper oxide catalysts. *J. Colloid Interface Sci.* **2011**, *357*, 497–503. [CrossRef] [PubMed]

30. Fornasiero, P.; Dimonte, R.; Rao, G.R.; Kaspar, J.; Meriani, S.; Trovarelli, A.; Graziani, M. Rh-loaded CeO2-ZrO2 solid-solutions as highly efficient oxygen exchangers: Dependence of the reduction behavior and the oxygen storage capacity on the structural-properties. *J. Catal.* **1995**, *151*, 168–177. [CrossRef]
31. Ganduglia-Pirovano, M.V.; Hofmann, A.; Sauer, J. Oxygen vacancies in transition metal and rare earth oxides: Current state of understanding and remaining challenges. *Surf. Sci. Rep.* **2007**, *62*, 219–270. [CrossRef]
32. Yu, Y.-Y.; Gong, X.-Q. CO oxidation at rutile TiO2 (110): Role of oxygen vacancies and titanium interstitials. *ACS Catal.* **2015**, *5*, 2042–2050. [CrossRef]
33. Li, H.; Guo, Y.; Robertson, J. Calculation of TiO2 surface and subsurface oxygen vacancy by the screened exchange functional. *J. Phys. Chem. C* **2015**, *119*, 18160–18166. [CrossRef]
34. Malakooti, R.; Mahmoudi, H.; Hosseinabadi, R.; Petrov, S.; Migliori, A. Facile synthesis of pure non-monoclinic zirconia nanoparticles and their catalytic activity investigations for Knoevenagel condensation. *RSC Adv.* **2013**, *44*, 22353–22359. [CrossRef]
35. Ahmad, W.; Noor, T.; Zeeshan, M. Effect of synthesis route on catalytic properties andperformance of Co3O4/TiO2 for carbon monoxide and hydrocarbon oxidation under real engine operating conditions. *Catal. Commun.* **2017**, *89*, 19–24. [CrossRef]
36. Yang, Y.; Huang, K.; Liu, R.; Wang, L.; Zeng, W.; Zhang, P. Shape-controlled synthesis of nanocubic Co3O4 by hydrothermal oxidation method. *Trans. Nonferrous Met. Soc. China* **2007**, *17*, 1082–1086. [CrossRef]
37. Matsumoto, S.I. Recent advances in automobile exhaust catalysts. *Catal. Today* **2004**, *3–4*, 183–190. [CrossRef]
38. Vera, D.; Crossan, M. Improvisation and innovative performance in teams. *Organ. Sci.* **2005**, *3*, 203–224. [CrossRef]
39. Li, W.; Nie, X.; Jiang, X.; Zhang, A.; Ding, F.; Liu, M.; Liu, Z.; Guo, X.; Song, C. ZrO2 support imparts superior activity and stability of Co catalysts for CO2 methanation. *Appl. Catal. B Environ.* **2018**, *220*, 397–408. [CrossRef]
40. Li, P.; Chen, X.; Li, Y.; Schwank, J.W. A review on oxygen storage capacity of CeO2-based materials Influence factors, measurement techniques, and applications in reactions related to catalytic automotive emissions control. *Catal. Today* **2019**, *327*, 90–115. [CrossRef]
41. Priya, N.S.; Somayaji, C.; Kanagaraj, S. Optimization of ceria-zirconia solid solution based on OSC measurement by cyclic heating process. *Procedia Eng.* **2013**, *64*, 1235–1241. [CrossRef]
42. Jigish, J.G.; Pravin, P.R.; Krunal, P.S. Exhaust Analysis of C.I Engine by Using Zirconium Dioxide Coated Wire Mesh Catalytic Converter. *Int. J. Sci. Res. Dev.* **2014**, *1*, 763–766.
43. Zhao, Y.; Sohn, H.; Hu, B.; Niklas, J.; Poluektov, O.G.; Tian, J.; Delferro, M.; Hock, A.S. Zirconium Modification Promotes Catalytic Activity of a Single-Site Cobalt Heterogeneous Catalyst for Propane Dehydrogenation. *ACS Omega* **2018**, *3*, 11117–11127. [CrossRef]
44. Zhang, H.; Ruan, S.; Feng, C.; Xu, B.; Chen, W.; Dong, W. Photoelectric Properties of TiO2-ZrO2 Thin Films Prepared by Sol-Gel Method. *J. Nanosci. Nanotechnol.* **2011**, *11*, 10003–10006. [CrossRef]
45. Viinikainen, T.; Rönkkönen, H.; Bradshaw, H.; Stephenson, H.; Airaksinen, S.; Reinikainen, M.; Simell, P.; Krause, O. Acidic and basic surface sites of zirconia-based biomass gasification gas clean-up catalysts. *Appl. Catal. A Gen.* **2009**, *362*, 169–177. [CrossRef]
46. Yu, J.J.; Cheng, J.; Ma, C.Y.; Wang, H.L.; Li, L.D.; Hao, Z.P.; Xu, Z.P. NOx decomposition, storage and reduction over novel mixed oxide catalysts derived from hydrotalcite-like compounds. *J. Colloid Interface Sci.* **2009**, *333*, 423–430. [CrossRef] [PubMed]
47. Amin, C.M.; Chavda, K.; Gadhia, U. Exhaust analysis of four stroke single cylinder diesel engine using copper based catalytic converter. *Int. J. Sci. Res. Dev.* **2013**, *1*, 493–497.
48. Reiter, M.S.; Kockelman, K.M. The problem of cold starts: A closer look at mobile source emissions levels. *Transp. Res. Part D Transp. Environ.* **2016**, *43*, 123–132. [CrossRef]
49. Paresh, D.P.; Pradip, M.P.; Nimesh, A.P.; Dhanajay, D.V. Experimental Investigation on Exhaust Emission with & Without MOLY Coated Piston Ring in C. I. Engine. *Int. J. Sci. Res. Dev.* **2014**, *1*, 570–573.

© 2020 by the authors. Licensee MDPI, Basel, Switzerland. This article is an open access article distributed under the terms and conditions of the Creative Commons Attribution (CC BY) license (http://creativecommons.org/licenses/by/4.0/).